

# ATMOSPHERIC CORRECTION ITERATIVE METHOD FOR HIGH RESOLUTION AEROSPACE IMAGING SPECTROMETERS

Alessandro Barducci, Donatella Guzzi, Paolo Marcoianni, Ivan Pippi\*

CNR – IFAC

Via Madonna del Piano 10, 50019 Sesto Fiorentino, ITALY

Tel.: +39 0555226301, Fax: +39 0555226348, \*e-mail: [L.Pippi@ifac.cnr.it](mailto:L.Pippi@ifac.cnr.it)

**KEY WORDS:** Atmospheric Correction, Imaging Spectrometers, Remote Sensing, Hyper Spectral Images, Environmental Monitoring.

## ABSTRACT:

The increasing radiometric accuracy and spectral resolution of the new aerospace optical imagers for Earth observation could allow a better characterization of the environment. This is true if accurate radiometric calibrations of the sensor are performed and atmospheric effects on the acquired data are carefully accounted for. To obtain spectral surface reflectance maps from the at-sensor radiance images, an improved atmospheric correction procedure have to be implemented. The availability of data acquired at high spectral resolution allows the detection of different spectral features of many atmospheric constituents. An iterative estimation algorithm based on high resolution data has been developed using the MODTRAN 4 radiative transfer code. The default atmospheric profiles available in that code have been firstly refined through at-ground level measurements of some parameters, like temperature, pressure, humidity, and solar irradiance. Then an iterative procedure has been started tuning H<sub>2</sub>O, CO<sub>2</sub>, CO, O<sub>3</sub>, and aerosol abundances. The MODTRAN 4 code is executed several times with different atmospheric parameters (H<sub>2</sub>O, CO<sub>2</sub>, CO, O<sub>3</sub>, and aerosol abundances) until the calculated ground irradiance matches the in-field measurements and the estimated ground spectral reflectance map is free from the related spectral signatures. To test and validate the method both simulated and acquired at-sensor radiance images have been utilized. The acquired images have been collected on 15th December 2005 during a coastal zone remote sensing campaign by the new airborne sensor HYPER / SIM-GA. The sensor has been operating in the 0.4 – 2.5  $\mu\text{m}$  spectral range with 768 bands and a resolution of 2.4 in the Visible Near Infra-Red (VNIR) and 5.4 nm in the Short Wave Infra-Red (SWIR). First results are presented and discussed taking into account the feasibility of avoiding in-field measurements.

## 1. INTRODUCTION

A satisfactory modelling of radiative transfer in the Earth's atmosphere (Kaufman, 1982; Golden, 1999; Thome, 1988; Kaufman, 1982; Gao, 2000) is requested when retrieving Level 2 remote sensed products from hyperspectral data acquired with aerospace sensors. Atmospherically corrected surface reflectance maps, for instance, improve the accuracy of target classification and are the starting point for estimating the radiation budget of the Earth and various biophysical parameters such as, fraction of absorbed photosynthetically active radiation (FPAR), leaf area index (LAI) and so forth that are retrieved by vegetation indices like the Normalized Difference Vegetation Index (NDVI) or the Photochemical Reflectance Index (PRI).

In many fields, such as agriculture and resource management, natural hazard investigation and disaster monitoring, there is a growing request of surface reflectance images that require atmospheric correction. In most of cases the adopted solution is based upon simple physical assumptions for which the effect of scattering is considered mainly as a pure additive term to the radiance reflected from the target and directly transmitted to the sensor. This "path radiance" term contains only those photons which are backscattered, in a large-angle scattering event (LAS event), from the atmosphere into the instantaneous field-of-view of the imaging sensor, mainly due to molecules (Rayleigh scattering) and small aerosols particles. From a radiometric point of view, this term has the effect to reduce the observed pixel spectrum in contrast (Vermote, 1997, Solomon, 1998; Tanrè, 1997).

If we want to take account multiple radiative interactions between the surface and the atmosphere (for example the effects of light trapping) together with small angle scattering events (SAS event), it is necessary to adopt a solution to the radiative transfer equation (RTE) (Tanrè, 1997; Tanrè, 1981; Barducci, 1994) starting from the following assumptions: (i) the light polarization is neglected; (ii) the atmosphere and the aerosols are horizontally stratified and optically thin; (iii) the atmosphere and the radiation field are stationary; (iv) the ground is a Lambert's reflector.

The at-sensor radiance coming from a specific site is also affected by atmospheric scattering from adjacent areas, by both "cross-talk" events and trapping effects, at an extent that depends on several factors such as sensor point spread function (PSF), scattering optical thickness, environment albedo and so forth. Hence, this effect must be taken into account to properly determine surface reflectance spectra (Barducci, 2002).

An atmospheric estimation iterative method for high resolution aerospace imaging spectrometers which is illustrated here as follows and some results are shown starting from high resolution hyperspectral images gathered by the new hyperspectral sensor HYPER / SIM-GA developed by Galileo Avionica.

## 2. DESCRIPTION OF ATMOSPHERIC CORRECTION MODELLING

### 2.1 Atmospheric correction method

In modelling the radiance propagation, the atmosphere is assumed to be a plane parallel medium (Tanrè, 1996; Wang, 1993; Gordon, 1997) whose description requires:

- the absorption and scattering coefficients  $\sigma_{abs}(z)$ ,  $\sigma_{sca}(z)$ , as a function of altitude  $z$ ,
- the scattering phase function representing the overall effect of the aerosols and dust particles  $\omega_0(\lambda, z)$

Neglecting the effects of polarization, according to the “scalar approximation” (Mekler, 1982; Wang, 1994; Ackerman, 1997), the propagation of electromagnetic radiation through the medium obeys the following RTE:

$$\frac{dL(\lambda, z, \xi)}{\sigma_{ext}(\lambda, z)dz} = -L(\lambda, z, \xi) + J(\lambda, z, \xi) \quad (1)$$

where  $L(\lambda, z, \xi)$  is the radiance, and  $J(\lambda, z, \xi)$  is the scattering source function which contains the contributions diffusely transmitted by the atmosphere within the sensor’s instantaneous field-of-view. We suppose both the atmosphere and the radiation field to be uniform over any horizontal planes.

From the above discussed hypotheses and taking an optically thin atmosphere, it follows that the light can be scattered only once, hence the RTE may be solved by using the “successive-order” method (Barducci, 2002):

$$L(\lambda, z; \xi) = L^{(0)}(\lambda, z, \xi) + L^{(1)}(\lambda, z, \xi) \quad (2)$$

where  $L^{(0)}(\lambda, z, \xi)$  represents the direct radiance and  $L^{(1)}(\lambda, z, \xi)$  is the radiance scattered once. According to the above assumptions supposing the neighbouring surface being spectrally similar to the central pixel, characterized by an average reflectance, we have:

$$L_{IB}(\lambda, z) = \frac{E(\lambda)}{\pi} \rho(\lambda) T(\lambda) + \frac{E(\lambda)}{\pi} \rho(\lambda) f(z, \theta) T(\lambda) \sec \theta \sigma_{sca}(\lambda) + L_{path}(\lambda, \theta) \quad (3)$$

Where  $\theta$  is the zenith angle,  $L_{IB}(\theta, \lambda)$  is the radiance reaching the sensor,  $E(\lambda)$  is the irradiance impinging on the target,  $T_s(\lambda)$  is the transmittance of the atmosphere which is supposed to be plane-parallel,  $\rho(\lambda)$  is the surface reflectance in the viewing direction  $\theta$  (the angle between the nadir and the viewing direction).  $L_{path}(\theta, \lambda)$  is the atmospheric path radiance and  $f(z, \theta)$  contains geometrical factors.

Inverting the above equation and putting in evidence the dependence of the scattering coefficient on wavelength, an expression for the reflectance spectrum is obtained:

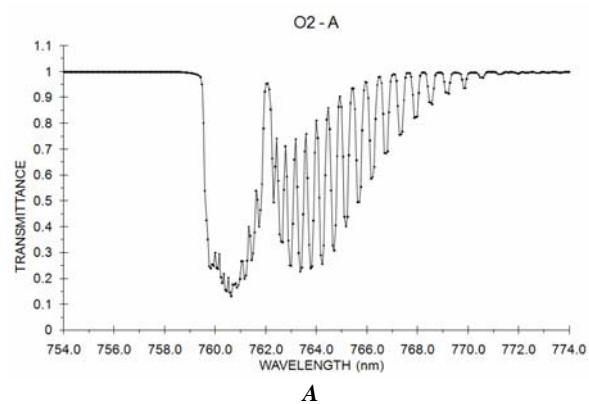
$$\rho(\lambda, \theta) = \frac{\pi[L_{IB}(x, y, \lambda) - L_{path}(\lambda, \theta)]}{E(\lambda)} \frac{1}{[T(\lambda) + \frac{A(z, \theta)}{2} \frac{1}{\lambda^\alpha} T(\lambda)^{\beta(\theta)}]} \quad (4)$$

Let us note that the Solar irradiance  $E(\lambda)$  impinging on the surface is multiplied by a spectral term containing the scattering coefficient and the atmospheric transmittance augmented by a geometric factor which takes into account the sensor instantaneous field-of-view.

## 2.2 Autonomous atmospheric retrieval

Parameterisation of aerosol optical thickness (or visibility), atmospheric water vapour content and other atmospheric constituents like  $O_3$  and  $CO_2$  requires atmospheric data that is often missing, while the acquisition parameters on observation geometry are usually known. The autonomous algorithm for retrieving the abundance of some atmospheric constituents is based on the assumption that telluric absorption lines should not be found in the retrieved spectral reflectance. On the other hand, errors on the abundance of atmospheric gasses propagate through the above equations, hence corrupting the estimated reflectance. These estimation errors are usually concentrated around the central wavelength of the considered absorption feature, introducing false absorption or emission bands in the apparent reflectance. Therefore, the smoothness of the retrieved reflectance in selected spectral regions is employed as key parameter for choosing the best atmospheric parametrization. In this way it is possible to estimate the abundance of important atmospheric constituents, such as  $CO_2$ ,  $CO$ ,  $H_2O$  vapour, and  $O_3$ . Estimation is performed using the Solvopt numerical optimisation procedure, which minimizes the roughness of the apparent reflectance by changing the above atmospheric abundances.

Retrieval of gas abundances using strong absorption bands may be affected by the saturation of the lines which form the bands, an effect that does not allow the exact retrieval of the desired abundances. For this reason an important feature is the spectral resolution, which must be sufficient to resolve the atmospheric lines. Figure 1 shows a comparison of the simulation of the atmospheric transmittance in the  $O_2$  A-band made at different spectral resolutions. In particular, results obtained with the new MODTRAN-5 radiative transfer code are compared with the ones obtained with the old MODTRAN-4 release. MODTRAN-5 has increased spectral resolution up to  $0.1 \text{ cm}^{-1}$ . This resolution better resolve the “depth” of the atmospheric absorbing lines.



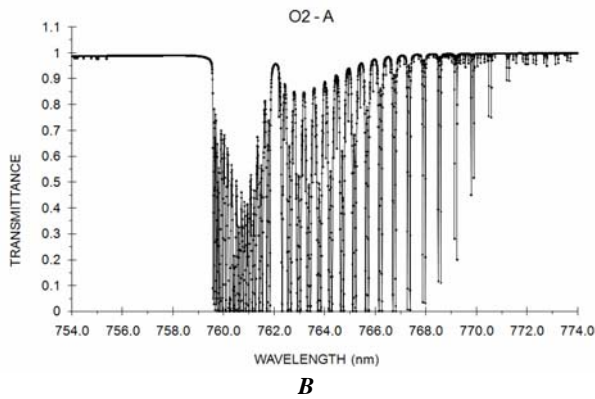


Figure 1. Typical mid-latitude summer atmospheric transmittance at O<sub>2</sub> A absorption band simulated at different spectral resolution: (A) 2 cm<sup>-1</sup> (MODTRAN-4 highest resolution), (B) 0.1 cm<sup>-1</sup> (MODTRAN-5 highest resolution). Higher resolution is needed for a correct modelling of the “depth” of the absorbing lines

Basically, the atmospheric estimation method is unable to retrieve the visibility and the aerosol loading. In order to overcome this important limitation our algorithm accepts as additional constraints the solar irradiance spectrum arriving at a fixed ground location and one or more reflectance spectra acquired on reference pixels within the image. Given this information, the iterative procedure based on the minimization of a cost function under the above constraints is employed to obtain information on the aerosol loading, the visibility, as well as the amount of some gaseous atmospheric constituents like water vapour, carbon dioxide, carbon monoxide and ozone.

### 3. DATA PROCESSING AND IMAGES

#### 3.1 Utilised airborne sensor

The HYPER/SIM-GA airborne sensor is a push-broom imaging spectrometer operating from the visible to the short wave infrared (SWIR) in the range 0.4 – 2.5 micron with 768 spectral bands and a resolution of 2.4 nm in the VNIR and 5.4 nm in the SWIR. The spectral properties of the sensor are described in Table 1 together with details about spatial resolution, spatial sampling interval and radiometric performance.

Sensor	HYPER/SIM-GA	
Type:	push-broom	
Sensor Head	VNIR	SWIR
Number of channels	512	256
Fiel of View	38°	24°
IFOV:	0.7°	1.3°
Spatial resolution:	1m	2m
Spectral range	400 – 1000nm	1000 – 2500nm
Spectral resolution	2.4nm	5.4nm
Quantisation accuracy:	12 bit	12 bit
SNR	50	50

Table1. Technical characteristics of HYPER/SIM-GA imaging sensor.

#### 3.2 The remote sensing campaign

On December 15, 2005, a CASA 220 airplane equipped with HYPER/SIM-GA was flown at a height of 1500 m and 3000 m a.s.l. The flight was performed around 11:00 A.M. (GMT), from North - North West toward South - South East, over the Tuscany coast (ITALY).

The overflight took about two hours during which some in-field measurements were performed to validate the remotely sensed spectra. In field measurements were made with different instruments in the San Rossore natural park. A portable spectrophotometer acquiring reflectance spectra and a portable spectro-irradiometer measuring the down-welling solar irradiance were used. The following set of atmospheric parameters has been acquired:

- air temperature, pressure, and relative humidity
- solar total irradiance (VIS and IR),
- solar spectral irradiance (VIS and NIR)
- CO<sub>2</sub> and H<sub>2</sub>O concentration at the top of forestry canopy level,
- spectral reflectance of natural surfaces.

The HYPER/SIM-GA dark signal was collected during the flight. The ancillary data have been subsequently used in order to improve the radiometric calibration of the sensor and to perform better atmospheric corrections.

#### 3.3 Analysis of simulated data

The algorithm was tested on a set of 3 synthetic images (dimension 256x256), formed of 389 spectral channels in the range 0.4 – 2.5 micron. The images are related to the same scene, characterized by different values of visibility and water vapor content. In figure 2 we report the simulated at sensor radiance extracted from 6 different pixels. In the figure is also shown the image of 153<sup>rd</sup> spectral channel.

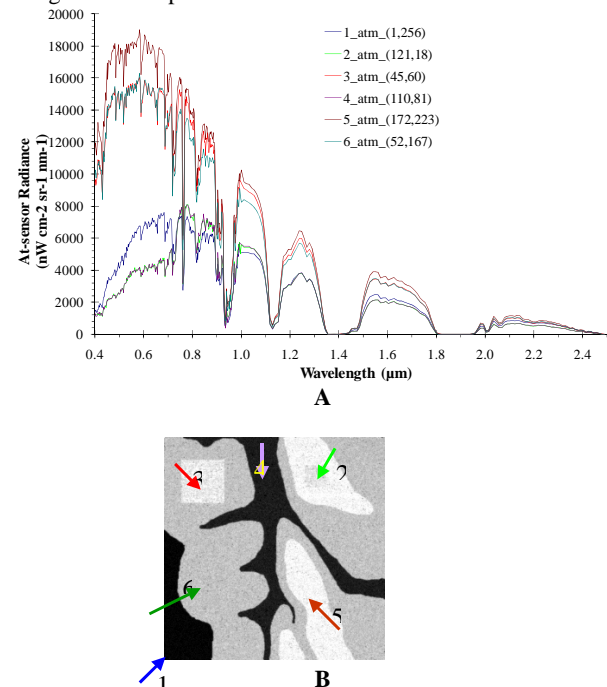


Figure 2. (A) At sensor radiance spectra of 6 different pixels extracted from a simulated clay scenario. The image of the 153<sup>rd</sup> channel is reported in (B). The pixels related to the extracted spectra are shown .

The atmospheric estimation algorithm was applied to the previous image constraining the calculation to the spectral irradiance revealed in a fixed pixel. The results are shown in Figure 3 where the retrieved and the ground truth reflectance measurements are shown.

The percentage error on the retrieved spectra is less than 10% with the exception of the first spectral channels. The value of atmospheric parameter retrieved by the procedure are shown in table II. In the same table their theoretical values used for the simulation of the image data are shown too. We point out that the algorithm result strongly depends on the data spectral resolution.

More specifically if the spectral resolution of MODTRAN 4 and image spectra are not accurately matched a relevant null-mean ripple is produced in spectral regions of high atmospheric absorption, as shown in Figure 3. It is interesting that this disturbance does not affect the estimation algorithm, which uses wavelength integral quantities that are free from this ripple. The algorithm estimation of aerosol loading is still unsatisfactory.

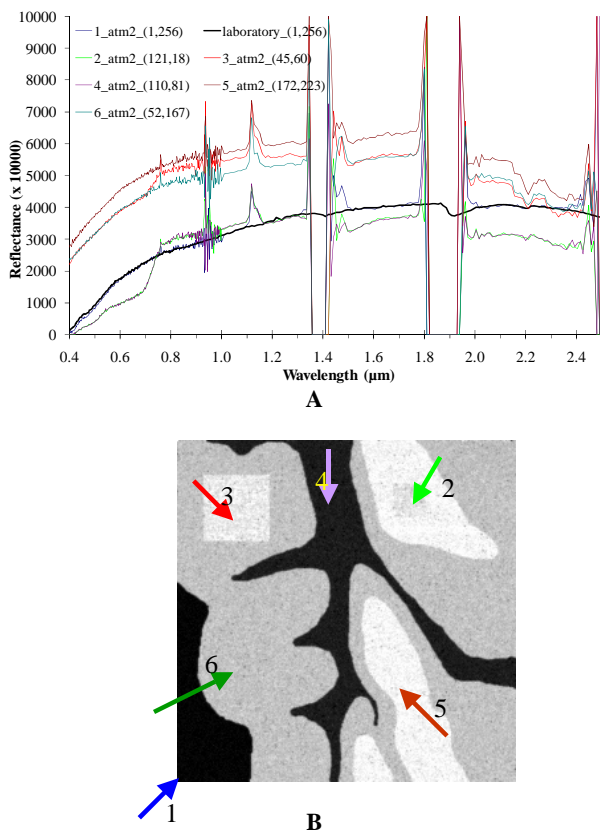


Figure 3. (A) Reflectance spectra of 6 different pixels extracted from a simulated clay scenario. A reference reflectance spectra is also shown. The image of the 153<sup>rd</sup> channel together with the pixels related to the extracted spectra are reported in (B).

	Theoretical Values	Retrieved Values
Visibility	23 km	19 km
H <sub>2</sub> O	2.9 g cm <sup>-2</sup>	2.8 g cm <sup>-2</sup>
CO <sub>2</sub>	439.5ppm	439.5ppm

Table 2. Comparison between theoretical and retrieved atmospheric parameters

### 3.4 Acquired data analysis

Remotely sensed data pre-processing was aimed to produce radiance calibrated images, according to the following scheme.

1. dark signal subtraction;
2. conversion to radiance unit (nW cm<sup>-2</sup> strad<sup>-1</sup> nm<sup>-1</sup>);
3. geometric correction and image geolocation.

This pre-processing produces a first level of calibrated remote sensing data useful for our research: the at-sensor radiance.

Figure 4 shows a HYPER/ SIM-GA composite images of San Rossore natural park radiometrically calibrated data for the VNIR (a) and SWIR spectrometers after the atmospheric correction phase.

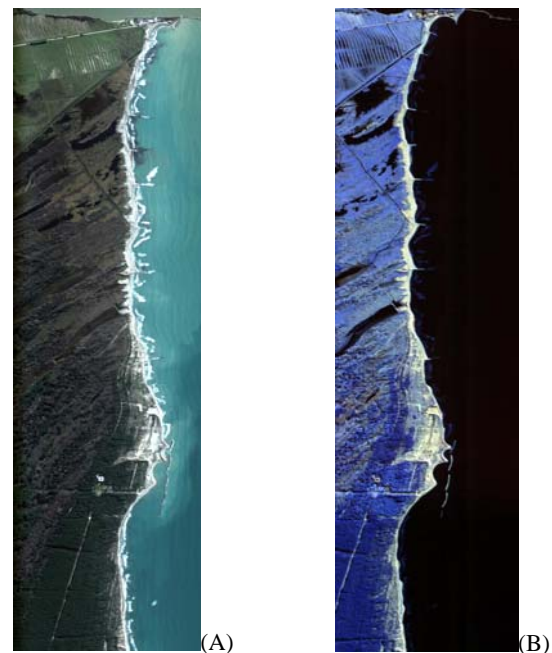


Figure 4. (A) True colour image (Red: 198<sup>th</sup> channel, Green: 153<sup>rd</sup> channel, Blue: 102<sup>nd</sup> channel) of the spectral reflectance acquired with HYPER SIM-GA VNIR sensor over the San Rossore natural Park. (B) Color composite (Red: 2227 nm, Green: 1565 nm, Blue: 1249 nm channel) of the spectral reflectance acquired with SWIR sensor over the same area. The reflectance maps of the observed scene have been processed with the new algorithm

In Figure 5 some reflectance spectra for different targets (green-grass, sand and water sea) are shown and compared with the reflectance measured in-situ for the same target.

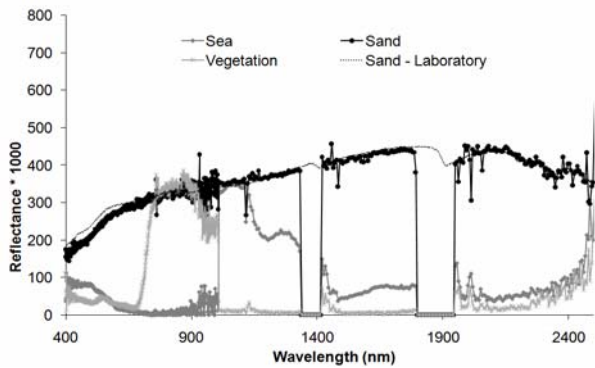


Figure 5. Reflectance spectra extracted from the HYPER SIM-GA VNIR and SWIR images presented in Fig.3 over forest, sand, and sea water. Sand reflectance spectrum measured in laboratory is also shown for comparison.

Remotely sensed spectra of Figure 5 show a good agreement with laboratory and in field data. However, a residual error with 10-15% of relative amplitude remains, hence producing a difference between the retrieved and measured reflectance spectrum at the same wavelength.

The use of MODTRAN 5, characterized by an increased spectral resolution, could improve the retrieved spectral reflectance.

#### 4. CONCLUDING REMARKS

In this paper an atmospheric correction method has been developed which help to correct remotely sensed data from the atmospheric effects. The method adopts the MODTRAN 4 code for atmospheric modelling and it was applied to simulated data and images acquired by the hyperspectral HYPER-SIMGA sensor. The algorithm has been tested with fair results. The main limitation to the application of this new data correction model is connected with the high spectral resolution required.

#### REFERENCES

Ackerman A., 1997. Remote sensing aerosols using satellite infrared observations, *Journal of Geophysical Research*, 102 (D14), pp. 17069-17079.

Barducci A. and I. Pippi, 1994. Small-angle atmospheric scattering of the light: outline of a theoretical model for adjacent effects on image remote sensing, *SPIE* 2312, pp. 74-84.

Barducci A., D. Guzzi, P. Marcoianni, I. Pippi, 2002. Atmospheric effects on hyperspectral data acquired with aerospace imaging spectrometers, *SPIE* 4884, pp. 1-9.

Gao B. -C. et al., 2000. Atmospheric Correction Algorithm for Hyperspectral Remote Sensing of Ocean Color from Space, *Applied Optics*, 39, pp. 887-896.

Golden A., G. P. Anderson *et al.*, 1999. Atmospheric Correction for Short-Wave Spectral Imagery Based on Modtran4, *SPIE Proc. Imaging Spectrometry V*, 3753, pp. 61-69.

Gordon H. R. , 1997. Atmospheric correction of ocean color imagery in the Earth Observing System, *Journal of Geophysical Research*, 102 (D14), pp. 17081-17106.

Kaufman Y., 1982. Solution of the Equation of Radiative Transfer for Remote Sensing Over Nonuniform Surface Reflectivity, *Journal of Geophysical Research*, 87(6), pp. 4137-4147.

Kaufman Y., D. Tanrè et al., 1997. Passive remote sensing of tropospheric aerosol and atmospheric correction for the aerosol effect, *Journal of Geophysical Research*, 102 (D14), pp. 16815-16830.

Mekler Y. and Y. Kaufman, 1982. Contrast reduction by the atmosphere and retrieval of nonuniform surface reflectance, *Applied Optics*, 21 (2), pp. 310-316.

Thome K. et al., 1988. Atmospheric Correction of ASTER, *IEEE Transactions on Geoscience and Remote Sensing*, 36 (4), pp. 1199-1211.

Solomon S. et al., 1998. Absorption of solar radiation by water vapor, oxygen, and related collisions pairs in the Earth's atmosphere, *Journal of Geophysical Research*, 103 (D4), pp. 3847-3858.

Tanrè D., M. Herman and P. Y. Deschamps, 1981. Influence of the background contribution upon space measurements of ground reflectance, *Applied Optics*, 20 (20), pp. 3678-3684.

Tanrè D., M. Herman and Y. Kaufman, 1996. Information on aerosol size distribution contained in solar reflected spectral radiances, *Journal of Geophysical Research*, 102 (D14), pp. 19043-19060.

Tanrè D., Y. Kaufman et al., 1997. Remote sensing of aerosol properties over oceans using the MODIS/EOS spectral radiances, *Journal of Geophysical Research*, 102 (D14), pp. 16971-16988.

Vermote E. F., Y. Kaufman et al., 1997. Atmospheric correction of visible to middle-infrared EOS-MODIS data over land surfaces: background, operational algorithm and validation, *Journal of Geophysical Research*, 102( D14), pp. 17131-17141.

Wang M. and H. R. Gordon, 1993. Retrieval of the columnar aerosol phase function and single-scattering albedo from sky radiance over the ocean: simulations, *Applied Optics*, 32 (24), pp. 4598-4609.

Wang M. and H. R. Gordon, 1994. Estimating aerosol optical properties over the oceans with the multiangle imaging spectroradiometer: some preliminary studies, *Applied Optics*, 33 (18), pp. 4042-4057.

